Journal of Advanced Research (2012) 3, 65–71

Cairo University

Journal of Advanced Research

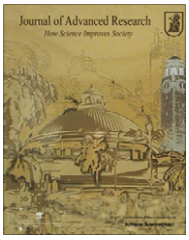

ORIGINAL ARTICLE

Platinum nanoparticles–manganese oxide nanorods as novel binary catalysts for formic acid oxidation

Mohamed S. El-Deab *

Department of Chemistry, Faculty of Science, Cairo University, Cairo, Egypt

Received 23 November 2010; revised 14 February 2011; accepted 4 April 2011
Available online 12 May 2011

KEYWORDS

Nanostructures;
Electrocatalysis;
CO oxidation;
Manganese oxides;
Binary catalysts

Abstract The current study proposes a novel binary catalyst system (composed of metal/metal oxide nanoparticles) as a promising electrocatalyst in formic acid oxidation. The electro-catalytic oxidation of formic acid is carried out with binary catalysts of Pt nanoparticles (nano-Pt) and manganese oxide nanorods (nano-MnO_x) electrodeposited onto glassy carbon (GC) electrodes. Cyclic voltammetric (CV) measurements showed that unmodified GC and nano-MnO_x/GC electrodes have no catalytic activity. While two oxidation peaks were observed at nano-Pt/GC electrode at ca. 0.2 and 0.55 V (corresponding to the direct oxidation of formic acid and the oxidation of the poisoning CO intermediate, respectively). The combined use of nano-MnO_x and nano-Pt results in superb enhancement of the direct oxidation pathway. Nano-MnO_x is shown to facilitate the oxidation of CO (to CO_2) by providing oxygen at low over-potential. This leads to retrieval of Pt active sites necessary for the direct oxidation of formic acid. The higher catalytic activity of nano-MnO_x/nano-Pt/GC electrode (with Pt firstly deposited) compared to its *mirror image* electrode (i.e., with MnO_x firstly deposited, nano-Pt/nano-MnO_x/GC) reveals that the order of the electrodeposition is an essential parameter.

Introduction

Catalysis and electrocatalysis at nanoparticles' surfaces is a subject of continuously growing interest due to its diverse applications [1–5]. The incentive behind this interest is attributed to the fascinating properties of the nanoparticles in addition to the use of minute amounts compared to the bulk material. Metal (or metal oxide) nanoparticles are usually dispersed and confined onto a relatively inert substrate, e.g., glassy carbon (GC). For instance, Au nanoparticles-based catalysts are widely applicable in many vital processes, e.g., reduction of NO with propene, CO or H_2, removal of CO from H_2 streams, selective oxidation, e.g., epoxidation of olefins as well as selective hydrogenation of CO and CO_2 [6–9].

* Tel.: +202 3567 6603; fax: +202 3752 7556.
E-mail address: msaada68@yahoo.com

Peer review under responsibility of Cairo University.
doi:10.1016/j.jare.2011.04.002

ELSEVIER Production and hosting by Elsevier

Au nanoparticle-based electrodes showed an extraordinary catalytic activity for the oxygen reduction [2,3,10,11] and have been efficiently utilized for the hydrogenation of unsaturated organics [12,13] as well as low-temperature oxidation of CO [14,15].

Electrochemical deposition [16–18] as well as several chemical techniques such as sol-gel [19], deposition from colloidal suspension [20] are currently in use for the preparation of different metal and metal oxide nanoparticles of various geometries, morphologies and dimensions. The electrochemical deposition technique is among the most familiar binder-free techniques used for the fabrication of nanostructures because of the facile control of the characteristics of the metal (or the metal oxide) nanoparticles (e.g., mass, thickness, morphology, etc.) by adjusting the current density, bath chemistry and temperature [17,21].

The use of Pt bi-metallic nanostructured catalysts had been suggested for the efficient oxidation of formic acid [22–25]. Moreover, the combined use of metal (e.g., Au, Pt or Pd) and metal oxide (e.g., MnO_x, Fe_3O_4, Co_3O_4, or NiO_x) nanostructures (e.g., nanotubes, nanorods and nanoparticles [26–28]) as binary catalysts had been suggested for several applications including the oxygen reduction reaction (ORR), the catalytic hydrogenation of unsaturated alcohols and aldehydes as well as the electro-oxidation of methanol [29,30]. The superb synergistic effect of the two components of the binary catalyst might arise from the momentarily consecutive (electro-) chemical reactions taking place at each constitute of the binary catalyst. For instance, the combined use of MnO_x and Au nanoparticles resulted in the occurrence of the ORR at a potential similar to that obtained at Pt electrodes, supporting an apparent 4-electron reduction pathway [30,31]. Thus, the proper design (by adjusting the amount and/or the order of preparation) of the binary catalyst is of prime importance to maximize the catalytic activity toward the desired reaction on the one hand and to reduce the amount of the precious metal on the other.

In the present study, a novel nanoparticles-based binary catalyst composed of Pt and manganese oxide (MnO_x) directly electrodeposited onto GC is suggested for the efficient electrooxidation of formic acid. MnO_x has been chosen as a second component in the proposed catalyst with an aim to provide oxygen species to enhance the oxidation process of formic acid. The influence of the order of electrodeposition of the two species onto GC electrodes on the electrocatalytic oxidation of formic acid is investigated aiming at maximization of the catalytic performance on one hand, and to reduce the amount of the precious metal on the other hand.

Experimental

The working electrode is a GC rod (ϕ = 5.0 mm, in diameter) sealed in a Teflon jacket leaving an exposed geometric surface area of 0.2 cm^2. In some experiments Pt electrode (ϕ = 2.0 mm, in diameter) is used as the working electrode. A spiral Pt wire and a saturated calomel electrode (SCE) were the counter and the reference electrodes, respectively. GC and Pt electrodes were mechanically polished with No. 2000 emery paper, then with aqueous slurries of successively finer alumina powder (down to 0.05 μm) with the help of a polishing microcloth, and then sonicated for 10 min in Milli-Q water. The polished Pt electrode is then electrochemically pretreated in deaerated 0.1 M H_2SO_4 by cycling the potential between −0.3 and 1.25 V vs. SCE at 50 mV s^{-1} for 10 min or until a reproducible cyclic voltammogram (CV) characteristic for a clean Pt electrode was obtained, cf. curve a in Fig. 5B. Pt nanoparticles were electrodeposited on the thus-prepared GC electrodes (nano-Pt/GC) from an acidic solution of 0.1 M H_2SO_4 containing 2.0 mM H_2PtCl_6. Potential step electrolysis from 1 to 0.1 V vs. SCE for 300 s was utilized to perform the electrodeposition of the Pt nanoparticles resulting in the electrodeposition of 3.3 μg of Pt (estimated from the charge of the *i-t* curve). Whereas, manganese oxide nanorods (nano-MnO_x) are electrodeposited onto the GC, nano-Pt/GC and Pt electrodes from a solution of 0.1 M Na_2SO_4 containing 0.1 M $Mn(CH_3COO)_2$ by applying 25 potential cycles between −0.05 and 0.35 V vs. SCE at 20 mV s^{-1}. XRD and high resolution TEM data [32] revealed the electrodeposition of the nanorods in the (1 1 $\bar{1}$) single crystalline manganite phase (γ-MnOOH). The surface coverage θ of nano-MnO_x on nano-Pt/GC and Pt electrodes has been estimated from the decrease of the peak current intensity around 0.4 V corresponding to the reduction of the Pt surface oxide monolayer formed during the anodic scan, cf. Fig. 2.

Scanning electron microscopy (SEM) imaging of the Pt (and/or MnO_x) nanoparticles electrodeposited onto the GC electrodes was carried out using a field emission scanning electron microscope (Hitachi S-5200 FE-SEM) at an acceleration voltage of 10 kV and a working distance of 4–5 mm.

The electrocatalytic activity of the nanoparticles-based MnO_x-Pt binary catalyst modified GC electrodes toward formic acid oxidation is examined in a deaerated solution of 0.3 M formic acid of pH 3.45 (adjusted by NaOH). CV measurements are carried out in a conventional three-electrode glass cell. All chemicals are Suprapur® grade; all measurements are performed at room temperature. Current densities are calculated on the basis of the geometric surface area of the GC working electrode; the solutions are de-oxygenated by N_2 bubbling.

Results and discussion

Morphological and electrochemical characterization

Fig. 1 shows SEM micrographs obtained for (A) nano-MnO_x/GC, (B) nano-Pt/GC, (C) nano-Pt/nano-MnO_x/GC and (D) nano-MnO_x/nano-Pt/GC electrodes. The MnO_x was electrodeposited in a porous texture composed of nanorods onto the GC electrode surface (image A). This texture covers homogeneously the entire surface of the GC electrode. On the other hand, round-shape Pt nanoparticles (particle size of ca. 10–100 nm) are electrodeposited at bare GC (image B) and nano-MnO_x modified GC (image C) electrodes. Image D reveals the electrodeposition of nano-MnO_x onto the Pt nanoparticles rather than at the bare portion of the GC electrode.

Fig. 2A shows CVs of (a) unmodified GC, (b) nano-Pt/GC and (b) nano-MnO_x/nano-Pt/GC electrodes in 0.1 M H_2SO_4 at a scan rate of 50 mV s^{-1}. In curve b, the formation of the Pt surface oxide and its reduction (at ca. 400 mV) reflects the successful electrodeposition of the Pt nanoparticles. The real surface area of nano-Pt is estimated from the charge consumed during the reduction of Pt-oxide monolayer using a reported value of 420 μC cm^{-2} [33]. The electrodeposition of nano-MnO_x onto this electrode resulted in a significant

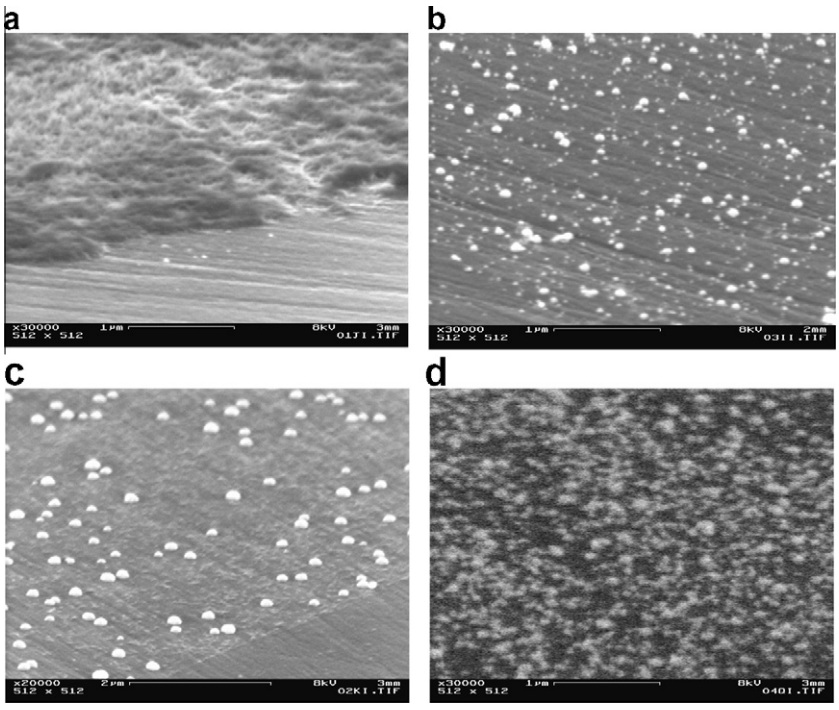

Fig. 1 SEM images obtained for (a) nano-MnO_x/GC, (b) nano-Pt/GC, (c) nano-Pt/nano-MnO_x/GC and (d) nano-MnO_x/nano-Pt/GC electrodes. MnO_x nanoparticles were electrodeposited from 0.1 M Na_2SO_4 + 0.1 $Mn(CH_3COO)_2$ by applying 25 potential cycles between −0.05 and 0.35 V vs. SCE at 20 mV s^{-1}. The Pt nanoparticles were electrodeposited from 0.1 M H_2SO_4 containing 2.0 mM H_2PtCl_6 by applying 300 s potential step electrolysis from 1 to 0.1 V vs. SCE. Note that image c corresponds to the sequential electrodeposition of nano-MnO_x followed by nano-Pt onto GC electrode and image d corresponds to the opposite order of electrodeposition.

decrease in the accessible surface area of the electrodeposited nano-Pt as revealed from the decrease of the reduction peak current at ca. 400 mV ($\theta \approx 46\%$). Fig. 2B shows CVs of (a) unmodified GC, (b) nano-MnO_x/GC and (c) nano-Pt/nano-MnO_x/GC electrodes in 0.1 M H_2SO_4 at a scan rate of 50 mV s^{-1}. Note that nano-Pt is electrodeposited onto nano-MnO_x/GC electrode in curve c of Fig. 2B. The appearance of a reduction peak of Pt oxide (at ca. 400 mV) in addition to the observation of small hydrogen adsorption–desorption peaks reveal the electrodeposition of Pt onto the nano-MnO_x modified GC electrode (curve c).

Electrocatalytic activity toward formic acid oxidation

The electrocatalytic behavior of the various nano-MnO_x/nano-Pt/GC electrodes toward formic acid oxidation is followed by CVs in a deaerated solution of 0.3 M formic acid (pH 3.45) as shown in Fig. 3. Note that a steady-state CV spectrum is observed after the second scan (shown in this figure). This figure shows the following interesting points:

(i) GC electrode has no catalytic activity toward formic acid oxidation (curve a). The electrodeposition of minute amount of nano-Pt (curve b) resulted in the observation of two oxidation peaks for formic acid similar to the behavior of bulk Pt electrode [34].
(ii) The first peak (at ca. 0.2 V) is attributed to the direct oxidation of formic acid to CO_2, and the second one (at ca. 0.55 V) is assigned to the oxidation of the adsorbed CO (produced as a dehydration oxidation product of formic acid).
(iii) Interestingly, the electrodeposition of nano-MnO_x onto nano-Pt/GC electrode (curve c) resulted in a significant enhancement of the current of the first peak (corresponding to the direct oxidation of formic acid) with a concurrent depression of the second peak. This indicates that less amount of CO is produced at the surface. Alternatively, one might attribute the observed enhancing effect to the oxidation of CO at less anodic potential at the nano-MnO_x modified electrode compared to the unmodified one (cf. Fig. 6A).
(iv) In Fig. 3 (curve b, i.e., for nano-Pt/GC electrode) the two peaks appeared during the anodic (forward) scan are usually assigned to the direct oxidation of formic acid to CO_2 and the oxidation of the poisoning intermediate CO to CO_2 at ca. 0.2 and 0.5 V, respectively.
(v) Likewise, during the backward scan, the two peaks are apparently assigned to the same two reactions with higher catalytic activity. In other words, the catalytic activity in the forward direction is less than that observed during the backward scan. This might arise from the fact that the catalytic activity of the unmodified Pt is controlled by a high surface coverage of CO_{ad} in the anodic sweep, while it is controlled by a high surface coverage of OH_{ad} during the reverse scan.
(vi) On the other hand, the catalytic activity of the nano-MnO_x/nano-Pt/GC electrode (Fig. 3, curve c) toward formic acid oxidation in the cathodic and anodic sweep directions are comparable; approaching the similar behavior observed at Pd-based catalysts. This indicates the high catalytic ability of this electrode toward the direct oxidation of formic acid (to CO_2) during the

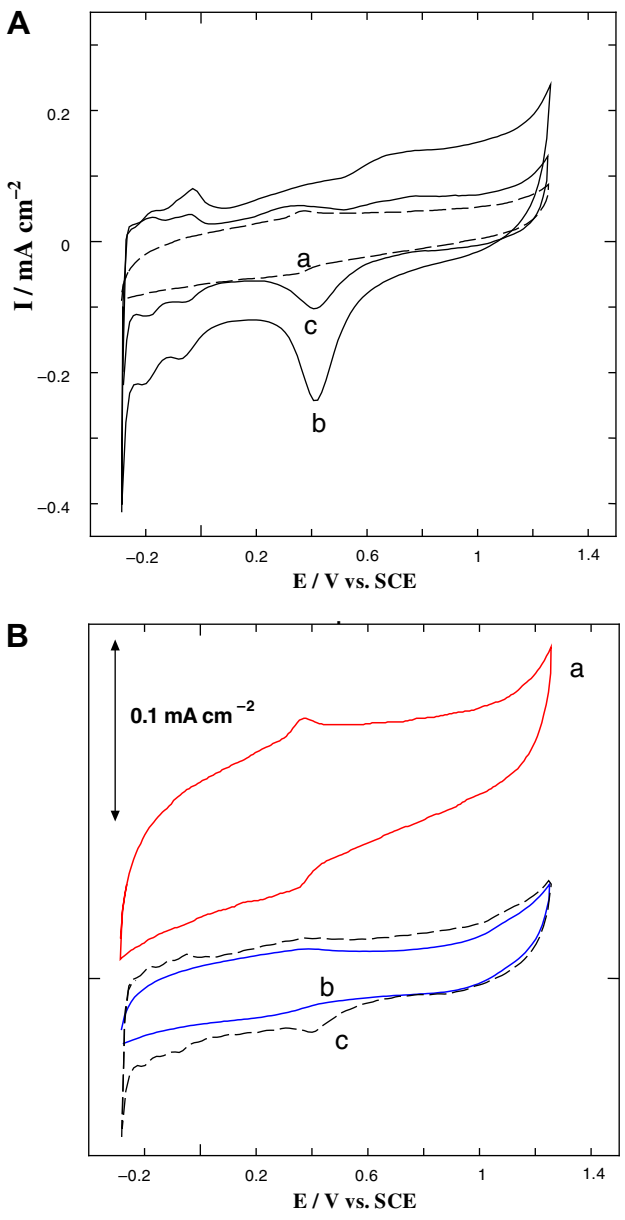

Fig. 2 (A) CVs obtained for (a) unmodified GC, (b) nano-Pt/GC and (c) nano-MnO_x/nano-Pt/GC electrodes ($\theta \approx 46\%$) and (B) CVs obtained for (a) unmodified GC, (b) nano-MnO_x/GC and (c) nano-Pt/nano-MnO_x/GC electrodes (ϕ = 5.0 mm) in deaerated 0.1 M H_2SO_4. Potential scan rate: 50 mV s^{-1}. The electrodeposition conditions used for MnO_x and Pt nanoparticles are the same as in Fig. 1.

forward as well as the backward scan directions as reflected by the depression of the second oxidation peak (at ca. 0.5 V) with a concurrent enhancement of the first oxidation peak (at ca. 0.2 V).

(vii) The absence of the oxidation peak at ca. 0.5 V (during the backward scan at this electrode) with no CO at the surface indicates the inherent relation of this peak and CO oxidation to CO_2.

It is thus interesting to investigate the effect of the order of electrodeposition of nano-Pt and nano-MnO_x on the

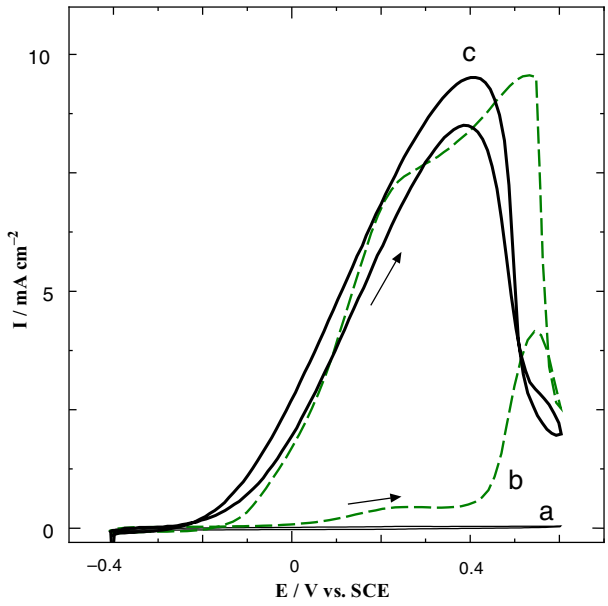

Fig. 3 CVs for formic acid oxidation at (a) unmodified GC, (b) nano-Pt/GC and (c) nano-MnO_x/nano-Pt/GC ($\theta \approx 46\%$) electrodes in 0.3 M HCOOH (pH 3.45) at 50 mV s^{-1}. The electrodeposition conditions used for MnO_x and Pt nanoparticles are the same as in Fig. 1.

electrocatalytic performance toward formic acid oxidation. Fig. 4 shows CVs of nano-MnO_x modified GC (curve b) compared to unmodified GC (curve a). This figure indicates that the nano-MnO_x does not induce any significant catalytic activity toward formic acid oxidation (curve b). The

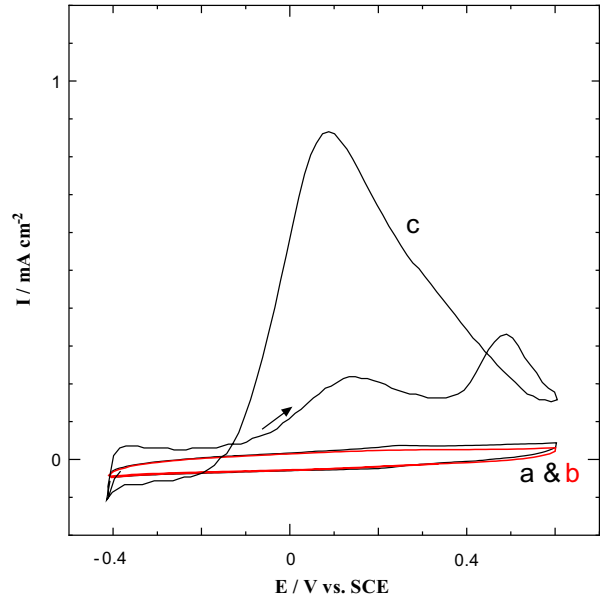

Fig. 4 CVs for formic acid oxidation at (a) unmodified GC, (b) nano-MnO_x/GC and (c) nano-Pt/nano-MnO_x/GC electrodes in 0.3 M HCOOH (pH 3.45) at 50 mV s^{-1}. The electrodeposition conditions used for MnO_x and Pt nanoparticles are the same as in Fig. 1.

electrodeposition of nano-Pt (as a second step of modification) onto nano-MnO_x/GC electrode (curve c) resulted in the appearance of two oxidation peaks at ca. 0.2 and 0.55 V similar (albeit with lower peak current intensities) to those observed at nano-Pt/GC electrode, see curve b in Fig. 3. The higher catalytic activity of the nano-MnO_x/nano-Pt/GC electrode, see curve c in Fig. 3, compared to its *mirror image* nano-Pt/nano-MnO_x/GC electrode, curve c of Fig. 4, reveals the importance of the sequence of electrodeposition of Pt and MnO_x. Thus the design of the binary catalyst is crucial for obtaining a catalytically active electrode toward the desired reaction. This design-dependent catalytic activity is shown for the oxygen reduction reaction (ORR) at Au nanoparticles–MnO_x nanorods binary catalyst [30].

Role of MnO_x

It has been generally reported that formic acid oxidation at Pt group metals proceeds according to reaction Scheme 1 [35]. According to this scheme the direct oxidation path (k_d) resulted in CO_2 (through a reactive intermediate, presumably formate radical [36]) and the poison formation path (k_p) resulted in CO due to a *nonfaradaic* dehydration of formic acid [36]. The latter can effectively block the Pt active sites of the surface and thus hinders the formation of OH_{ad} (k_{OH}) required to keep the catalyst in an active state.

Inspection of Fig. 4 (curve b) reveals that nano-MnO_x is not sufficient to catalyze (or initiate) the reaction at GC electrode, indicating the necessity of Pt for the initiation of formic acid oxidation as it provides a suitable base for formic acid adsorption. However, the generation of the poisoning CO (as a dehydration product) blocks the active surface sites of Pt and impedes the complete oxidation of formic acid; see curve b in Fig. 3. Thus, Pt alone is not sufficient to catalyze the direct oxidation reaction at a reasonable rate, mainly because of the surface poisoning by CO. The complete oxidation of CO to CO_2 requires the availability of oxygen at low potentials.

Investigating the effect of soluble Mn^{2+} ions on the catalytic behavior of unmodified Pt electrode has been carried out to proof the exclusive essential role of the prepared MnO_x toward formic acid oxidation and to probe the possibility of homogeneous catalysis of Mn^{2+} ions (if any). The effect of soluble Mn^{2+} ions on the catalytic enhancement toward formic acid oxidation is shown in Fig. 5A. CVs are measured at unmodified Pt electrode in 0.3 M formic acid solution (pH 3.45) in the absence (a) and presence (b) of 0.4 mM Mn^{2+} ions. This figure does not show any significant enhancement of the catalytic activity of Pt in the presence of Mn^{2+} ions. This implies the necessity and involvement of MnO_x in the oxidation of formic acid. Fig. 5B shows CVs measured in 0.1 M H_2SO_4 for Pt electrode (a) before and (b) after measuring curve b of Fig. 5A. It shows that the presence of Mn^{2+} ions in the solution does not cause any significant change in the real surface area of Pt.

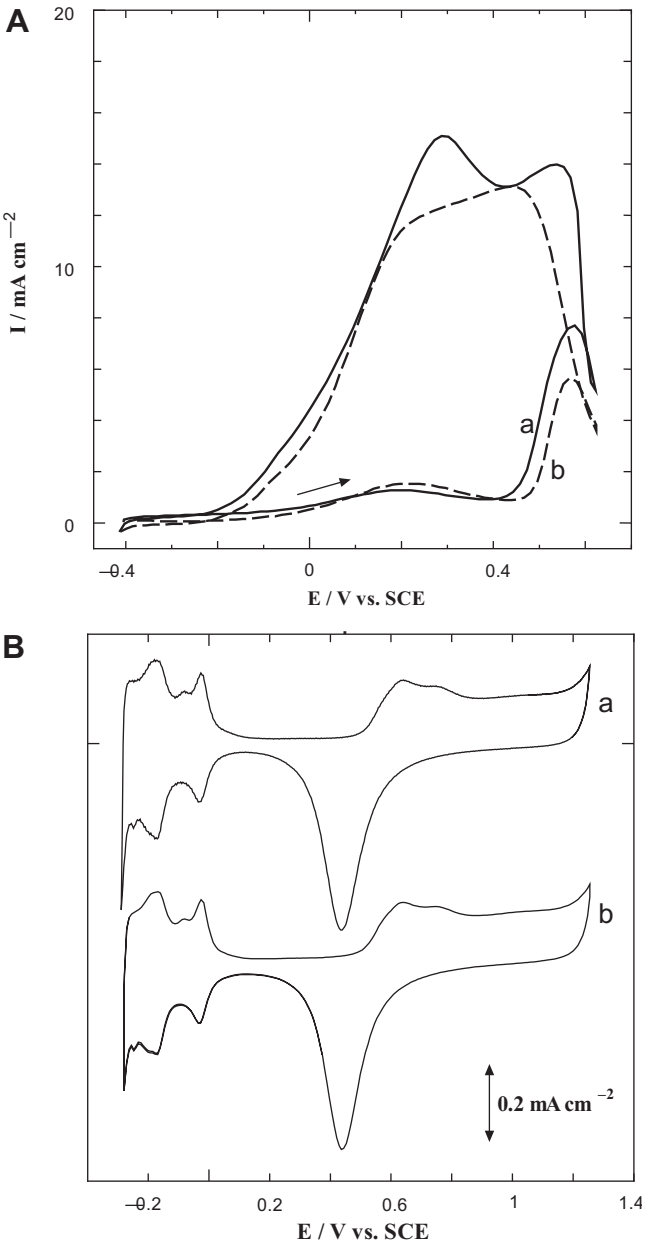

Fig. 5 (A) CVs for formic acid oxidation at unmodified Pt electrode (ϕ = 2.0 mm) in 0.3 M HCOOH (pH 3.45) in (a) the absence and (b) the presence of 0.4 mM Mn^{2+} ions. Potential scan rate: 50 mV s^{-1}. (B) CVs measured at unmodified Pt electrode in a deaerated 0.1 M H_2SO_4 (a) before and (b) after the measurement of curve b of Fig. 5A. Potential scan rate: 50 mV s^{-1}.

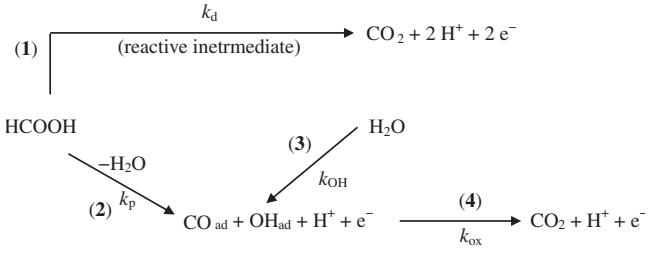

Scheme 1 Illustration of the possible oxidation pathways of formic acid at Pt surface.

The catalytic role of MnO_x can be attributed to: (i) mediated oxidation of formic acid to CO_2 without generating CO and/or (ii) mediated oxidation of the adsorbed CO species at the Pt active sites. In order to investigate the catalytic influence of MnO_x on the oxidation of CO, Fig. 6A shows oxidative

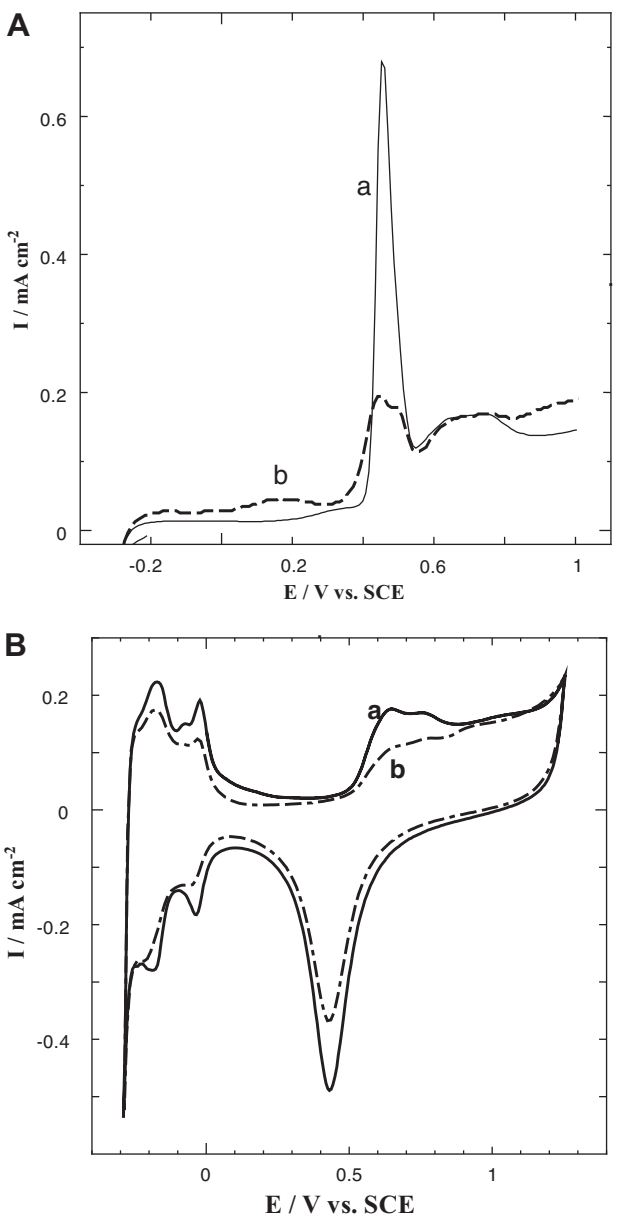

Fig. 6 (A) Linear sweep voltammograms (LSVs) for the oxidative stripping of CO adsorbed at (a) unmodified Pt and (b) nano-MnO_x/Pt ($\theta \approx 30\%$) in 0.1 M H_2SO_4. (B) CVs for (a) unmodified Pt and (b) nano-MnO_x/Pt ($\theta \approx 30\%$) electrodes in 0.1 M H_2SO_4 at potential scan rate of 50 mV s^{-1}. MnO_x nanoparticles are electrodeposited onto Pt electrode from 0.1 M Na_2SO_4 + 0.1 $Mn(CH_3COO)_2$ by applying 25 potential cycles between −0.05 and 0.35 V vs. SCE at 20 mV s^{-1}.

stripping voltammograms of CO adsorbed at: (a) unmodified Pt and (b) nano-MnO_x modified Pt electrodes. This figure shows that the onset of CO oxidation starts at a lower positive potential (ca. 0.18 V) at the nano-MnO_x/Pt electrode compared to the unmodified Pt (peak at 0.45 V). Fig. 6B shows a noticeable decrease of the Pt-oxide reduction peak (around 0.4 V) indicating the effective electrodeposition of nano-MnO_x. The favorable oxidation of CO is derived by the supply of oxygen species through a reversible redox transformation of MnOOH to MnO_2 according to [37] :

$$MnOOH + OH^- \leftrightarrow MnO_2 + H_2O + e^- \quad (1)$$

The produced MnO_2 (with a strong oxidizing power) is thought to provide oxygen and thus facilitate the oxidation of CO (adsorbed at Pt active sites) to CO_2, leading to retrieval of the Pt active sites (via removal of the poison) as:

$$MnO_2 + Pt\ldots CO_{ads} + OH^- \rightarrow MnOOH + CO_2 + Pt_{free} + e^- \quad (2)$$

where the term "Pt...CO_{ads}" refers to Pt active surface site blocked with adsorbed CO. Reaction (2) indicates the regeneration of the γ-MnOOH phase which is believed to act as a catalytic mediator facilitating the oxidation of CO into CO_2. The sequential coupling of Reactions (1) and (2) results, effectively, in the generation of CO_2 and retrieval of free Pt active surface sites as:

$$Pt\ldots CO_{ads} + 2OH^- \rightarrow CO_2 + Pt_{free} + H_2O + 2e^- \quad (3)$$

Thus, it can be argued that the origin of the catalytic role of nano-MnO_x toward formic acid oxidation originates from the enhanced CO oxidation by facilitating the oxygen supply through a reversible redox system of Mn(III)/(IV) oxides.

Conclusions

The current study addresses the electrocatalytic oxidation of formic acid at nanoparticles-based binary catalyst of Pt and manganese oxide. Neither Pt nor MnO_x can catalyze the direct oxidation process at a reasonable rate. The combined use of nano-Pt and nano-MnO_x (electrodeposition of Pt followed with MnO_x) resulted in the efficient electro-oxidation of formic acid to CO_2. Nano-Pt is considered a necessary component for the adsorption of formic acid (to initiate the oxidation process), while MnO_x acts as a catalytic mediator that facilitates the retrieval of the Pt active sites (blocked with the adsorbed CO generated as a dehydration oxidation product) through oxidation of the adsorbed poison (CO) to CO_2.

Acknowledgments

The author is grateful for the Alexander von Humboldt Foundation (Bonn, Germany) for the fellowship and for supporting his research stay at Institute of Electrochemistry, Ulm University, Ulm, Germany.

References

[1] Alexeyeva N, Tammeveski K. Electroreduction of oxygen on gold nanoparticle/PDDA-MWCNT nanocomposites in acid solution. Anal Chim Acta 2008;618(2):140–6.
[2] El-Deab MS, Sotomura T, Ohsaka T. Oxygen reduction at electrochemically deposited crystallographically oriented Au(1 0 0)-like gold nanoparticles. Electrochem Commun 2005;7(1):29–34.
[3] El-Deab MS, Ohsaka T. Hydrodynamic voltammetric studies of the oxygen reduction at gold nanoparticles-electrodeposited gold electrodes. Electrochim Acta 2002;47(26):4255–61.
[4] Tegou A, Papadimitriou S, Armyanov S, Valova E, Kokkinidis G, Sotiropoulos S. Oxygen reduction at platinum- and gold-coated iron, cobalt, nickel and lead deposits on glassy carbon substrates. J Electroanal Chem 2008;623(2):187–96.
[5] Li S, Yang W, Chen M, Gao J, Kang J, Qi Y. Preparation of PbO nanoparticles by microwave irradiation and their

application to Pb(II)-selective electrode based on cellulose acetate. Mater Chem Phys 2005;90(2–3):262–9.
[6] Qian L, Wang K, Fang H, Li Y, Ma X. Au nanoparticles enhance CO oxidation onto SnO_2 nanobelt. Mater Chem Phys 2007;103:132–6.
[7] Liu X, Wang A, Zhang T, Su D-S, Mou C-Y. Au–Cu alloy nanoparticles supported on silica gel as catalyst for CO oxidation: effects of Au/Cu ratios. Catal Today 2011;160:103–8.
[8] Llorca J, Domunguez M, Ledesma C, Chimento R, Medina F, Sueiras J, Angurell I, Seco M, Rossell O. Propene epoxidation over TiO_2-supported Au–Cu alloy catalysts prepared from thiol-capped nanoparticles. J Catal 2008;258:187–98.
[9] Lignier P, Comotti M, Schuth F, Rousset J-L, Caps V. Effect of the titania morphology on the Au/TiO_2-catalyzed aerobic epoxidation of stilbene. Catal Today 2009;141:355–60.
[10] Yang H, Coutanceau C, Leger J-M, Vante NA, Lamy C. Methanol tolerant oxygen reduction on carbon-supported Pt–Ni alloy nanoparticles. J Electroanal Chem 2005;576(2):305–13.
[11] Zhang Y, Asahina S, Yoshihara S, Shirakashi T. Oxygen reduction on Au nanoparticle deposited boron-doped diamond films. Electrochim Acta 2003;48(6):741–7.
[12] Pradhan N, Pal A, Pal T. Silver nanoparticle catalyzed reduction of aromatic nitro compounds. Colloids Surf A Physicochem Eng Asp 2002;196(2-3):247–57.
[13] Schimpf S, Lucas M, Mohr C, Rodemerck U, Bruckner A, Radnik J. Supported gold nanoparticles: in-depth catalyst characterization and application in hydrogenation and oxidation reactions. Catal Today 2002;72(1–2):63–78.
[14] Haruta M, Date M. Advances in the catalysis of Au nanoparticles. Appl Catal A Gen 2001;222(1-2):427–37.
[15] Haruta M. Size- and support-dependency in the catalysis of gold. Catal Today 1997;36(1):153–66.
[16] Finot MO, Braybrook GD, McDermott MT. Characterization of electrochemically deposited gold nanocrystals on glassy carbon electrodes. J Electroanal Chem 1999;466(2):234–41.
[17] El-Deab MS, Sotomura T, Ohsaka T. Size and crystallographic orientation controls of gold nanoparticles electrodeposited on GC electrodes. J Electrochem Soc 2005;152(1):C1–6.
[18] Jiang J, Kucernak A. Electrochemical supercapacitor material based on manganese oxide: preparation and characterization. Electrochim Acta 2002;47(15):2381–6.
[19] Lee HY, Kim SW, Lee HY. Expansion of active site area and improvement of kinetic reversibility in electrochemical pseudocapacitor electrode. Electrochem Solid-State Lett 2001;4(3):A19–22.
[20] Pang SC, Anderson MA, Chapman TW. Novel electrode materials for thin-film ultracapacitors: comparison of electrochemical properties of sol-gel-derived and electrodeposited manganese dioxide. J Electrochem Soc 2000;147(2):444–50.
[21] Srinivasan V, Weidner JW. An electrochemical route for making porous nickel oxide electrochemical capacitors. J Electrochem Soc 1997;144(8):L210–3.
[22] Li X, Hsing I-M. Electrooxidation of formic acid on carbon supported $Pt_x\ Pd_{1-x\ (x\ =\ 0–1)}$ nanocatalysts. Electrochim Acta 2006;51:3477–83.
[23] Waszczuk P, Barnard T, Rice C, Masel R, Wieckowski A. Nanoparticle catalyst with superior activity for electrooxidation of formic acid. Electrochem Commun 2002;4:599–603.
[24] Kristian N, Yan Y, Wang X. Highly efficient submonolayer Pt-decorated Au nano-catalysts for formic acid oxidation. Chem Commun 2008:353–5.
[25] Chen W, Kim J, Sun S, Chen S. Composition effects of FePt alloy nanoparticles on the electro-oxidation of formic acid. Langmuir 2007;23(22):11303–10.
[26] Jana NR, Gearheart L, Murphy CJ. Synthetic control of the diameter and length of single crystal semiconductor nanowires. J Phys Chem B 2001;105(19):4065–7.
[27] Kim F, Song JH, Yang P. Photochemical synthesis of gold nanorods. J Am Chem Soc 2002;124(48):14316–7.
[28] Malikova N, Santos IP, Schierhorn M, Kotov NA, Marzan LML. Layer-by-layer assembled mixed spherical and planar gold nanoparticles: control of interparticle interactions. Langmuir 2002;18(9):3694–7.
[29] Xu M-W, Gao G-Y, Zhou W-J, Zhang K-F, Li H-L. Novel Pd/β-MnO_2 nanotubes composites as catalysts for methanol oxidation in alkaline solution. J Power Sources 2008;175(1):217–20.
[30] El-Deab MS, Ohsaka T. Electrocatalytic reduction of oxygen at Au nanoparticles–manganese oxide nanoparticle binary catalysts. J Electrochem Soc 2006;153(7):A1365–71.
[31] El-Deab MS, Ohsaka T. Electrocatalysis by design: Effect of the loading level of Au nanoparticles–MnO_x nanoparticles binary catalysts on the electrochemical reduction of molecular oxygen. Electrochim Acta 2007;52(5):2166–74.
[32] El-Deab MS, Ohsaka T. Manganese oxide nanoparticles electrodeposited on platinum are superior to platinum for oxygen reduction. Angew Chem Int Ed 2006;45(36):5963–6.
[33] Trasatti S, Petrii OA. Real surface area measurements in electrochemistry. J Pure Appl Chem 1991;63:711–34.
[34] El-Deab MS, Kibler LA, Kolb DM. Enhanced electro-oxidation of formic acid at manganese oxide single crystalline nanorod modified Pt electrodes. Electrochem Commun 2009;11(4):776–8.
[35] Capon A, Parson R. The oxidation of formic acid on noble metal electrodes: II. A comparison of the behaviour of pure electrodes. J Electroanal Chem 1973;44(2):239–54.
[36] Markovic NM, Ross P. Surface science studies of model fuel cell electrocatalysts. Surf Sci Rep 2002;45(4-6):117–229.
[37] Pourbaix M. Atlas of electrochemical equilibria in aqueous solutions. Oxford: Pergamon Press; 1966.